Sustainable
Food Technology

ROYAL SOCIETY
OF CHEMISTRY

REVIEW

View Article Online
View Journal | View Issue

Check for updates

Cite this: *Sustainable Food Technol.*, 2025, **3**, 1705

Machine-learning driven design of bio-based active food packaging films with improved mechanical properties

Sanjeev Gautam, [*a] Monika Verma [ab] and Tarundeep Singh Lakhanpal[a]

Received 9th May 2025
Accepted 10th August 2025

DOI: 10.1039/d5fb00198f

rsc.li/susfoodtech

Bio-based active packaging films offer a sustainable route to replace petro-plastic laminates, but their multicomponent formulations complicate rational design. We report a machine-learning driven workflow that couples response surface methodology with artificial neural networks to optimise starch–chitosan films plasticised with glycerol, reinforced with beeswax and ZnO, and activated using citrus-peel extract. The hybrid model shrank the experimental search space by 65% and predicted tensile strength, the water-vapour transmission rate and antimicrobial efficacy with $R^2 > 0.94$. The optimal film delivered a tensile strength of 3.5 Mpascal, a 31% drop in water-vapour permeability and a >3 log CFU reduction against *E. coli*, while remaining fully soil-biodegradable within 45 days. Fourier-transform infrared spectra confirmed hydrogen-bond-mediated compatibility between polysaccharide chains and bioactives, explaining the improved mechanical integrity. This study demonstrates that data-guided optimisation can accelerate the development of high-performance, biodegradable packaging and provides a transferable framework for next-generation sustainable food-contact materials.

[a] *Advanced Functional Materials Lab, Dr SSB University Institute of Chemical Engineering & Technology, Panjab University, Chandigarh-160014, India*

[b] *Energy Research Centre, Panjab University, Chandigarh-160014, India. E-mail: sgautam@pu.ac.in; Tel: +91 97797 13212*

Sanjeev Gautam

Sanjeev Gautam heads the Advanced Functional Materials Lab at Panjab University, Chandigarh, India. He earned his PhD in condensed-matter physics from the university in 2007, and then managed grid computing for the CMS experiment at CERN. From 2007 to 2014, he held a Star Post-Doctoral Fellowship at the Korea Institute of Science and Technology, where he performed advanced research on nanomaterials and sustainable energy systems. With 25 years of research experience, Dr Gautam has authored over 200+ peer-reviewed publications and holds an h-index of 37+. He edited/authored 5 books, and 20+ book chapters. His work has attracted National And International Funding Across Nanotechnology, Sustainable Energy, Food Technology, Catalysis, and Environmental Safety. He has supervised seven PhD and forty master's students and serves on the editorial boards of Scientific Reports, Materials Letters, Materials Letters: X, and Heliyon. Dr Gautam's current research focuses on designing next-generation functional materials that support greener technologies in energy, environmental protection, and healthcare.

Monika Verma

Monika Verma is a research scholar (May 2023) affiliated with the Advanced Functional Materials Laboratory in the Energy Research Centre, Panjab University, Chandigarh. Her doctoral research focuses on enhancing photovoltaic efficiency through ion-beam techniques. She received her MSc in Physics (2022) from Panjab University, where she was awarded a gold medal and a DST-INSPIRE Fellowship, and earned her BSc (Hons.) in Physics from GD Goenka University, Gurugram. Her research interests include energy storage and conversion systems, two-dimensional (2D) materials, and nano-devices. She has authored 6 research articles and 3 book chapters in peer-reviewed international publications, and holds an h-index of 4 with 32 citations. She also mentors postgraduate/undergraduate researchers, and serves as a reviewer for journals including Scientific Reports, Materials Letters, etc.

Sustainability spotlight

Petro-plastic packaging generates ~79 Mt of persistent waste annually. Our machine-learning-optimised starch–chitosan films reduce this burden by providing a compostable barrier material sourced from abundant biopolymers and fruit-processing waste. The workflow slashes experimental resources by 65%, promoting eco-efficient R&D. Achieving industrial-grade tensile strength (3.5 MPa) and a 31% drop in water-vapour permeability, the films extend shelf-life while degrading fully in 45 days of soil burial-closing the materials loop in line with UN SDG 12 (Responsible Consumption and Production). Antimicrobial action against *E. coli* supports SDG 3 (Good Health) by improving food safety, and bio-based feedstocks underpin SDG 2 (Zero Hunger) through reduced post-harvest loss.

1 Introduction

The increasing demand for convenient, nutritious, and long-lasting processed foods has led to the development of advanced food packaging technologies.[1] New innovations, such as active, intelligent, and bioactive packaging, are designed not only to contain food but also to interact with it or its environment to enhance safety and quality.[2] In particular, active packaging-especially those that use natural antioxidants and antimicrobials-has gained importance due to its effectiveness in preserving the food's color, texture, sensory qualities, and extending its shelf life. The widespread use of petroleum-based plastics in industries like food packaging, household products, and medical applications are due to their strength, low cost, light weight, and excellent resistance to heat and chemicals.[1] However, these synthetic polymers are highly resistant to degradation due to chemicals, sunlight, and microorganisms, leading to ongoing environmental pollution and significant sustainability challenges.[3] As a result, the development of environmental friendly, biodegradable alternatives like bioplastics has become a crucial area of research. Bioplastics are made from renewable biological materials such as starch, cellulose, lignin, casein, and lipids, offering benefits like biodegradability, environmental safety, and reduced reliance on fossil fuels.[4] Among these materials, starch stands out due to its wide availability, low cost, and excellent film-forming properties. It can be sourced from various plants, including corn, potatoes, cassava, jackfruit seeds, mango seeds, avocado seeds, and sago.[2,5–8]

Starch-based films are non-toxic, transparent, colorless, and odorless, making them ideal for sustainable packaging solutions.[9] However, their high hydrophilicity limits water resistance and mechanical strength, restricting their practical applications.[10] To address these issues, plasticizers like glycerol are commonly used to reduce hydrogen bonding and enhance flexibility, with glycerol being favored for its stable hydroxyl interactions and lower volatility compared to alternatives like water or sorbitol.[11] Combining starch with co-polymers such as chitosan-derived from the deacetylation of chitin in crustacean shells-can significantly improve mechanical strength, water resistance, and antimicrobial properties. Chitosan's natural bioactivity and hydrophobic characteristics complement starch's film-forming ability, making starch–chitosan composites ideal for active food packaging.[12] Recent studies have also explored alternative starch sources like avocado and tamarind seeds, which are often overlooked agro-industrial byproducts rich in polysaccharides and proteins, presenting promising opportunities for edible and biodegradable films.[12] Tamarind seed starch, for example, has excellent film-forming potential, though its processing requires further optimization. To enhance the functionality of starch-based films, the addition of essential oils (EOs), such as clove essential oil (CEO), rich in eugenol and caryophyllene, provides antioxidant and antimicrobial benefits.[13,14] However, excessive amounts of spice extracts or EOs may affect nutrient absorption, highlighting the need for controlled formulation strategies. Additionally, fruit peels, especially from *Citrus sinensis* (sweet orange), are a significant source of natural antioxidants and antimicrobial compounds, with extracts from orange peels (OPE) demonstrating strong antibacterial properties and being effectively used in antimicrobial packaging films.[13]

The graph shown in Fig. 1(a) illustrates the adoption percentages of smart packaging solutions in two regions: the United States and Asia. It reveals that the United States leads with a 75% adoption rate, while Asia has a 60% rate. This suggests that smart packaging technologies are more readily accepted in the U.S. than in Asia, indicating a greater market readiness, consumer awareness, or technological infrastructure in the United States. Nevertheless, the 60% adoption rate in Asia signifies considerable growth and potential for the future development of smart packaging solutions in that region. Besides this, the United Kingdom captures 27% regional market share being a leading in European packaging industries while France, the world's most sustainable country expected the

Tarundeep Singh Lakhanpal

Tarundeep Singh Lakhanpal is pursuing a master's program in Food Technology at the University Institute of Chemical Engineering and Technology (UICET), Panjab University, Chandigarh, India. Since commencing his postgraduate studies in 2023, he has focused on investigating the application of Artificial Intelligence (AI) and Machine Learning (ML) to intelligently design biodegradable packaging films aimed at enhancing food shelf life. He holds a B.Tech. in Food Technology from Punjab Agricultural University, Ludhiana, India. Tarundeep is particularly passionate about integrating advanced concepts such as smart packaging solutions, predictive modeling, and data-driven approaches to develop sustainable, high-performance packaging systems that address global food preservation challenges.

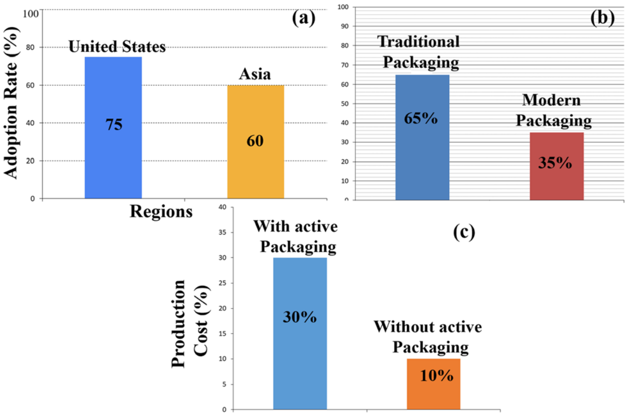

Fig. 1 (a) Adoption rates of smart packaging solutions, (b) consumer preferences: traditional *vs.* modern packaging, and (c) comparison of product costs with and without active packaging.

highest growth rate to be nearly 6% during 2024–2029. Conversely, in Africa and Latin America the adoption rate is below 50% due to lack of infrastructure and cost constraints.[15]

The graph given above in Fig. 1(b) reveals that 65% of consumers lean towards traditional packaging, in contrast to the 35% who prefer modern options. This suggests that, despite the progress and innovations in packaging technology, a significant portion of consumers continues to have confidence in and favor traditional formats. Furthermore, this underscores a possible obstacle to the swift acceptance of modern packaging solutions, indicating that businesses might need to enhance consumer education and awareness to address this disparity. The graph shown in Fig. 1(c) demonstrates that products utilizing active packaging incur substantially higher expenses, representing 30% of the overall product cost, in contrast to merely 10% for those without active packaging. This notable disparity underscores a significant economic obstacle to the broader implementation of active packaging technologies, as the elevated costs may dissuade both manufacturers and consumers, particularly in price-sensitive markets.

Despite the potential of natural biopolymers and active additives, the development of composite films using innovative combinations-such as avocado seed starch with orange peel extract (OPE), or soybean aqueous extract (SAE) combined with beeswax (BW) and emulsifiers like Span 20 (SP)-has not been fully explored. SAE, a protein-rich byproduct containing 7S and 11S globulins, forms strong film networks when heated and enhances antioxidant properties due to its isoflavone content.[13,16] To achieve optimal mechanical and functional properties, it is crucial to carefully adjust factors like starch concentration, plasticizer levels, temperature, and co-polymer ratios when formulating edible films. Traditional trial-and-error approaches are ineffective for these complex multivariable systems. Therefore, optimization methods like Response Surface Methodology (RSM) and Artificial Neural Networks (ANNs) have gained popularity. RSM offers a systematic statistical approach for experimental design, model development, and optimization by evaluating linear, quadratic, and interaction effects among independent variables (IV).[17] One key tool within RSM is the Central Composite Design (CCD), which allows for the effective analysis of complex parameter interactions. On the other hand, ANN models excel in capturing nonlinear relationships between inputs and outputs, providing better predictive accuracy for multifactorial systems.[18] In recent years, both ANNs and RSM have been applied to optimize the compositions of edible films, predicting properties like tensile strength, elongation at break, water vapor permeability, and antimicrobial effectiveness. ANN-based feedforward-backpropagation models, often implemented in MATLAB, have shown superior predictive accuracy and generalizability compared to traditional regression models.

This research combines the latest developments in bio-based packaging by creating biodegradable edible films through the use of various natural polymers, including corn starch, tamarind, avocado seed starch, soybean aqueous extract (SAE), and chitosan. It also incorporates plasticizers such as glycerol, lipids like beeswax, and bioactive additives including clove essential oil (CEO) and orange peel extract (OPE). To stabilize the lipid-protein matrix, emulsifiers such as Span 20 were added. The films were produced *via* the solution casting technique and optimized through Response Surface Methodology (RSM) utilizing a face-centered CCD and ANN modeling, as evidenced by similar optimization research.[19,20]

The predictive accuracy of the models was evaluated using error metrics and response surface plots. FTIR spectroscopy was employed to investigate the molecular interactions among the film components, confirming hydrogen bonding and compatibility between the biopolymers and additives.[21] A detailed characterization of the films was performed, assessing mechanical properties such as tensile strength (TS) and elongation at break (EAB), barrier properties like water vapor permeability (WVP), and moisture sensitivity indicators such as moisture content (MC) and water solubility (WS). Optical properties, including lightness (L), whiteness index (WI), yellowness index (YI), and opacity (OP), were also measured to evaluate the films' visual characteristics and functional effectiveness.[22,23] By incorporating biodegradable materials and bioactive compounds, this study supports the shift from synthetic plastics to sustainable alternatives. It not only improves understanding of edible film formulations but also highlights their potential in maintaining food safety and quality in modern packaging solutions.[24,25]

2 Types of AI and ML models

The fields of Artificial Intelligence (AI) and Machine Learning (ML) have experienced considerable growth in food packaging, especially in the creation of active and intelligent packaging systems. These sophisticated computational models allow researchers to examine intricate datasets, represent nonlinear relationships, and accurately forecast a material's characteristics.[26] Fig. 2 depicts several AI and ML models frequently utilized in food packaging research, highlighting their distinct functions and applications.

1. Response Surface Methodology (RSM) is a statistical approach used to model and optimize processes influenced by

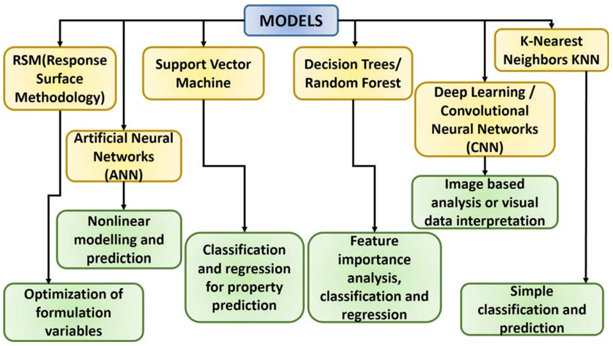

Fig. 2 Types of AI and ML models used in food technology to optimize formulations, predict quality, model complex processes, and improve efficiency while reducing experimental time and cost.

multiple variables. This technique helps in assessing the effects of independent variables and their interactions on one or more response variables (RVs) through structured experiments, such as Central Composite Design (CCD) and Box-Behnken Design (BBD).[27,28] RSM uses a second-order polynomial equation to analyze experimental data, allowing for the creation of response surface and contour plots that assist in optimization. This method reduces the number of experimental trials needed compared to full factorial designs while providing valuable insights into the process.[29] In food packaging and biopolymer research, RSM is widely used to improve film formulations by examining variables such as plasticizer concentrations, antimicrobial agents, and nanoparticles to enhance mechanical, barrier, and optical properties.[30] Its applications also extend to fields like analytical chemistry and other disciplines.[31]

2. Artificial Neural Networks (ANNs) are computational models inspired by the neural structure of the human brain. These networks consist of layers of interconnected nodes, or neurons, that process input data, identify patterns, and learn from examples. ANNs are particularly effective at capturing complex, nonlinear relationships between variables, making them ideal for tasks such as prediction, classification, and optimization.[32] In fields like food engineering, materials science, and biopolymer research, ANNs are used to predict properties like tensile strength, barrier characteristics, biodegradability, and shelf life based on formulation or processing parameters.[33] Unlike traditional statistical models, ANNs do not rely on predefined equations; instead, they learn directly from data through a training process. While Response Surface Methodology (RSM) provides clear visualizations and insights, ANNs typically offer superior accuracy in handling complex, nonlinear relationships.[34]

3. Support Vector Machine (SVM) is a supervised machine learning technique used for tasks like classification, regression, and outlier detection. The SVM algorithm identifies the optimal hyperplane that best separates different classes or predicts continuous outcomes with minimal error.[35] SVM is particularly known for its high accuracy, especially when the relationship between input variables and outcomes is nonlinear. This ability is enhanced by kernel functions, which transform input data into a higher-dimensional space to improve separability. In fields like food science, materials research, and packaging, SVM has been effectively used to predict film properties, assess quality attributes, and classify spoilage levels based on chemical, physical, or sensory data.[36] Compared to ANNs, SVM generally performs better with smaller datasets and reduces the risk of over-fitting through structural risk minimization.

4. Decision trees are supervised learning algorithms used for both classification and regression tasks. They work by splitting data into branches based on decision rules derived from input features, leading to predictions at the terminal nodes. Their simplicity and visual representation make them useful for analyzing the impact of individual variables.[37] However, individual decision trees are prone to overfitting and may become unstable over handling noisy datasets. To overcome these issues, the Random Forest (RF) algorithm was introduced. RF creates an ensemble of decision trees through bootstrap aggregation (bagging) and random feature selection, improving prediction accuracy and stability.[38] In food science, materials engineering, and biodegradable packaging, RF models are used to predict film properties, detect food spoilage or microbial contamination, and optimize formulations with complex datasets.[39] Random forest is particularly effective with high-dimensional, nonlinear data and provides variable importance scores to help with feature selection.

5. Deep Learning (DL) is a branch of machine learning that uses multi-layered neural networks to automatically detect complex patterns in large datasets. One of the most powerful architectures in deep learning is Convolutional Neural Networks (CNNs), which are particularly effective at processing image, spatial, and grid-like data.[40] CNNs are made up of layers that perform convolution, pooling, and activation functions, allowing the model to extract hierarchical features from raw input with minimal preprocessing. Although CNNs are mainly known for applications in image classification, object detection, and segmentation, their use is growing in areas like food quality evaluation, defect detection, and biomaterial surface analysis using imaging data.[41] In biopolymer packaging, CNNs and other deep learning methods are becoming valuable tools for assessing visual characteristics (such as opacity and surface roughness) and predicting performance based on image or high-dimensional sensory data.[42] While deep learning requires large datasets and significant computational power, it offers outstanding performance in solving complex, high-dimensional problems.

6. K-Nearest Neighbor (KNN) is a simple, non-parametric supervised learning algorithm used for both classification and regression tasks. The algorithm works by comparing a new data point to the '*k*' nearest data point in the training dataset, making predictions based on the majority class (for classification) or the average value (for regression) of its neighbors.[43] KNN is known for its simplicity, ease of implementation, and effectiveness with small to medium-sized datasets. However, its performance can be influenced by the choice of '*k*', the distance metric used, and the scaling of features. As the dataset size increases, KNN can become computationally expensive, as it requires storing and examining the entire training set during the prediction phase.[44] In fields such as food science, materials,

and packaging, KNN has been used to predict quality attributes, categorize product types, and detect spoilage based on chemical, mechanical, or image data. While it may not perform as well as deep learning for complex data, KNN remains a valuable tool for creating baseline models, rapid prototyping, and providing interpretable results.

3 Experimental design

RSM serves as a robust statistical instrument for designing, analyzing, and optimizing experiments that involve several variables. In the realm of food packaging research, especially concerning the creation of biodegradable and active films, RSM is instrumental in elucidating the interactions between ingredients and their effects on the properties of the films. The subsequent flowchart as shown in Fig. 3 delineates the methodical steps required to apply the RSM model, which includes defining objectives, selecting variables, validating the model, and implementing the optimized conditions.

The research examines four independent variables for the development of biodegradable edible films: Green Tea Extract (GTE), beeswax (BW), zinc oxide (ZnO), and glycerol (GLY). These variables are assessed within designated concentration ranges: GTE at 0.5% to 2%, beeswax at 0.5% to 1.5%, zinc oxide at 0.05% to 1%, and glycerol at 1% to 2%. Each variable is analyzed at five distinct levels to ensure the experimental design's robustness and rotatability. These levels consist of low (−1), indicating the minimum concentration within the specified range; medium (0), representing the midpoint; and high (+1), denoting the maximum concentration. Furthermore, two axial points, plus a $(+\alpha)$ and minus a $(-\alpha)$, are incorporated beyond the established range to improve the rotatability and reliability of the experimental framework.

1. Zinc oxide was chosen due to its antimicrobial characteristics, which contribute to prolonging the shelf life of food by preventing the proliferation of bacteria and fungi. Its integration into edible films provides improved defense against microbial contamination, an essential factor in food packaging.[45,46]

2. GTE was selected due to its antioxidant properties, containing polyphenols like catechins that neutralize free radicals and safeguard food against oxidative degradation. This contributes to preserving the freshness and nutritional integrity of packaged food.[47,48]

3. Beeswax acts as a water-repellent barrier, significantly decreasing the permeability of water vapor in the films. This improves the moisture resistance of the edible packaging, aiding in the preservation of food texture and quality by preventing the absorption or loss of excess moisture.[49,50]

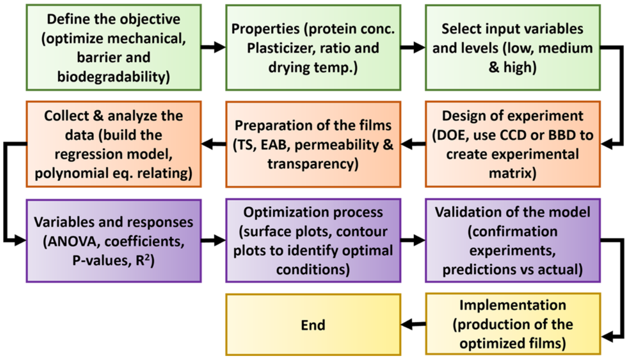

Fig. 3 Flowchart for response surface methodology.

3.1 Levels of each independent variable

A three-level factorial design was utilized to examine the impact of different formulation components on the characteristics of biodegradable edible films intended for active food packaging. This experimental approach facilitates the assessment of both the individual and interactive effects of the chosen factors on the response variables, as shown in Table 1.

In Table 1, the parameters, that is, the four factors-GTE, BW, ZnO, and GLY were tested at three levels: low (−1), medium (0), and high (+1). GTE, ranging from 0.5% to 2%, is included as an active ingredient with antioxidant and antimicrobial properties. BW, ranging from 0.5% to 1.5%, is used to enhance the hydrophobicity and barrier properties of the material. ZnO, tested between 0.05% and 1%, is incorporated for its antimicrobial and UV-blocking qualities, while GLY, ranging from 1% to 2%, serves as a plasticizer to improve the flexibility of the film or coating. These factors and their ranges reflect an experimental design, likely RSM, aimed at optimizing the formulation for optimal mechanical, barrier, and functional characteristics. The medium levels may help explore non-linear effects, and the overall goal is to create a biodegradable, active, and flexible material with enhanced performance.

3.2 CCD matrix

To enhance the formulation of biodegradable edible films that include functional bioactive and structural elements, a Central Composite Design (CCD) was employed. This design aids in the creation of predictive models by examining the linear, quadratic, and interaction effects of various variables on the targeted response characteristics which are shown in Tables 2 and 3, respectively.

3.2.1 Generalized coding for other factors. Similar calculations should be performed for BW, ZnO, and GLY using their respective ranges.

Tables 2 and 3 illustrate the experimental findings derived from the CCD matrix, which investigates the influence of GTE, BW, ZnO, and GLY on the properties of films. The tensile strength (TS) was observed to range between 2.14 MPa and 3.90 MPa, while the elongation at break (EAB) fluctuated from 142.55% to 205.61%, demonstrating the effects of these components on mechanical characteristics. The moisture content (MC) and water solubility (WS) exhibited significant variations, reflecting the roles of hydrophilic and hydrophobic elements. Water vapor permeability (WVP) was recorded to be between 2.33 and 3.99 g mm m^{-2} day kPa, indicating its impact on barrier properties. Additionally, optical characteristics such as the whiteness index (WI) (ranging from 45.99 to 73.66) and opacity (OP) (from 0.78 to 1.86) were affected by different

Table 1 Experimental factors

Factor	Low (−1) (minimum conc.)	Medium (0) (midpoint conc.)	High (+1) (maximum conc.)
Green tea extract (GTE)	0.5%	1.25%	2%
Beeswax (BW)	0.5%	1%	1.5%
Zinc oxide (ZnO)	0.05%	0.525%	1%
Glycerol (GLY)	1%	1.5%	2%

formulations. These findings underscore the significance of factor interactions in enhancing the mechanical, barrier, and optical attributes of biodegradable films.

3.2.2 Calculation of coded values for CCD. In a CCD, the coded values (Xi) for a factor are determined using the equation: $X_i = (A_i - A_{\text{center}})/\Delta A$. Here, A_i denotes the actual value of the factor at a specific level, A_{center} signifies the midpoint of the factor's range, and ΔA represents the step size, calculated as $\Delta A = (A_{\text{high}} - A_{\text{low}})/2$. In this scenario, A_{high} indicates the maximum actual value (associated with the +1 level), while A_{low} indicates the minimum actual value (linked to the −1 level). For instance, when considering Green Tea Extract (GTE), if A_{low} is 0.5%, A_{center} is 1.25%, and A_{high} is 2.0%, we can compute the step size ΔA as $\Delta A = (2.0 - 0.5\%)/2 = 0.75\%$. Utilizing this step size, the coded values for the various factor levels can subsequently be derived. The alpha ($\pm\alpha$) levels are established at ±0.25%, which correspond to the extreme factor levels of $-\alpha = 0.25\%$ and $+\alpha = 2.5\%$. Calculate step size ΔA

$$\Delta A = (2.0 - 0.5)/2 = 1.5/2 = 0.75$$

Computed coded values are shown in Table 4.

Table 4 presents the coded values for GTE across various levels. The actual GTE values range from 0.25% to 2.0%, with coded values derived from a span of 0.75. The minus alpha ($-\alpha$) level is associated with an actual GTE value of 0.25%, yielding a coded value of −1.33. The low (−1) level is defined at 0.5%, which corresponds to a coded value of −1. The center (0) value is established at 1.25%, resulting in a coded value of 0, while the high (+1) level is linked to an actual GTE value of 2.0%, with a coded value of +1.

3.3 Regression model polynomial equation

The response variable Y is defined by using the equation $Y = B_0 + B_1X_1 + B_2X_2 + B_3X_3 + B_{12}X_1X_2 + B_{13}X_1X_3 + B_{23}X_2X_3 + B_{21}X_1^2 + B_{22}X_2^2 + B_{23}X_3^2$. In this formulation, Y signifies the response variable, which may include TS, EAB, and WVP, among others. The variables affecting Y consist of X_1 (GTE), X_2 (BW), X_3 (ZnO), and X_4 (GLY). The constants B_0, B_1, B_2, B_3, and B_4 serve as the

Table 2 CCD matrix table with experimental results

Run	GTE	BW	ZnO	GLY	TS	EAB	MC	WS	WVP	WI	YI	L*	OP
1	0.00	0.000	0.000	0.00	2.75	185.07	19.71	31.83	4.01	44.97	71.95	84.25	1.01
2	−1.0	−1.00	−1.00	−1.0	3.90	142.55	24.93	30.07	3.51	63.73	76.12	70.04	1.39
3	−1.0	−1.00	1.000	1.00	3.46	156.29	18.48	38.43	2.89	53.75	48.95	74.94	1.39
4	0.00	0.000	1.682	0.00	3.20	162.97	30.73	31.35	2.33	59.77	39.17	71.02	1.25
5	0.00	1.682	0.000	0.00	2.31	171.05	21.62	30.21	2.85	72.13	44.71	70.70	0.63
6	1.00	1.000	−1.00	−1.0	2.52	170.15	30.60	26.13	3.98	70.42	38.69	81.74	1.19
7	1.00	−1.00	−1.00	−1.0	3.15	202.39	22.79	36.65	3.57	60.13	66.12	80.42	1.85
8	0.00	0.000	0.000	0.00	2.27	167.62	25.38	39.63	3.14	68.61	78.25	81.69	0.77
9	0.00	0.000	0.000	1.682	3.65	197.70	25.90	33.84	3.99	68.36	38.04	68.30	0.98
10	−1.0	−1.00	1.000	1.00	3.81	163.71	30.30	30.12	3.94	48.91	78.86	78.31	1.64

Table 3 CCD matrix table with experimental results (runs 11–20)

Run	GTE	BW	ZnO	GLY	TS	EAB	MC	WS	WVP	WI	YI	L*	OP
11	0.00	0.000	0.000	0.00	2.26	156.68	20.42	26.67	3.48	66.29	59.98	83.07	1.58
12	0.00	0.000	0.000	0.00	3.88	192.96	20.20	34.84	3.73	68.85	60.74	72.70	0.78
13	1.00	1.000	1.000	1.00	3.65	186.48	25.32	26.41	3.20	50.01	76.31	76.35	1.86
14	1.682	0.000	0.000	0.00	3.23	195.45	30.83	35.63	3.27	47.91	63.26	84.75	1.60
15	−1.68	0.000	0.000	0.00	3.12	185.42	25.12	29.56	3.34	55.80	74.84	66.87	1.23
16	−1.0	1.000	−1.00	1.00	3.95	174.42	25.08	30.76	2.58	72.36	69.48	70.33	1.69
17	−1.0	−1.00	1.000	−1.0	2.14	205.61	20.15	28.12	2.86	73.66	70.64	83.53	1.56
18	0.00	0.000	−1.68	0.00	2.92	191.50	27.89	29.25	3.49	45.99	79.89	71.65	1.75
19	0.00	0.000	0.000	−1.68	2.58	206.56	20.72	34.04	3.01	61.02	45.03	69.46	1.73
20	1.00	1.000	1.000	1.00	3.11	133.14	30.95	34.26	3.83	54.49	70.38	67.61	1.63

Table 4 Coded values for green tea extract (GTE)

Level	Actual value (%)	Coded value (X)
Minus alpha ($-\alpha$)	0.25	$(0.25 - 1.25)/0.75 = -1.33$
Low (−1)	0.5	$(0.5 - 1.25)/0.75 = -1$
Center (0)	1.25	$(1.25 - 1.25)/0.75 = 0$
High (+1)	2.0	$(2.0 - 1.25)/0.75 = 1$

linear coefficients for each respective factor, while B_{12}, B_{13}, B_{14}, B_{23}, B_{24}, and B_{34} represent the interaction coefficients for combinations of factors. The quadratic coefficients for each factor are indicated by ${B_1}^2$, ${B_2}^2$, ${B_3}^2$, and ${B_4}^2$.

3.4 ANOVA analysis of the RSM

Here is an example of analysis of variance (ANOVA) performed to discuss about one response that is tensile strength in the given Table 5, and similar calculations will be performed for the rest of the responses one by one and the ANOVA table will be formulated for each response respectively. Table 5 displays the results of the ANOVA concerning the influence of GTE, BW, ZnO, and GLY on the properties of the film, including their interactions. The p-values are utilized to assess the statistical significance of each individual factor and their interactions. The individual factors reveal non-significant results at the 0.05 level, with GTE ($p = 0.5158$), BW ($p = 0.2458$), ZnO ($p = 0.4995$), and GLY ($p = 0.0768$), the latter being the closest to significance. The squared terms (GTE^2, BW^2, ZnO^2, and GLY^2) also present non-significant p-values, indicating a lack of quadratic effects on the outcome. Likewise, the interactions, including GTE × BW ($p = 0.8009$) and GTE × ZnO ($p = 0.1644$), do not demonstrate significant effects. The residual variance, with a p-value of 0.5158, implies that the unexplained variability in the model is insufficient to indicate any significant unexplained effects. This indicates that, although the factors and their interactions may have some influence, they do not achieve statistical significance at the 0.05 level.

Table 5 ANOVA table

Source	Sum of squares	DF	F-value	p-Value
GTE	0.1641	1	0.4766	0.5158
BW	0.5695	1	1.6543	0.2458
ZnO	0.1777	1	0.5162	0.4995
GLY	1.5678	1	4.5538	0.0768
GTE^2	0.1978	1	0.5744	0.4772
BW^2	0.0302	1	0.0876	0.7772
ZnO^2	0.0974	1	0.2830	0.6138
GLY^2	0.1409	1	0.4093	0.5460
GTE × BW	0.0239	1	0.0695	0.8009
GTE × ZnO	0.8634	1	2.5078	0.1644
GTE × GLY	0.3805	1	1.1052	0.3336
BW × ZnO	0.0229	1	0.0664	0.8052
BW × GLY	0.0049	1	0.0141	0.9092
ZnO × GLY	0.1195	1	0.3472	0.5772
Residual	2.0657	6	0.4766	0.5158

3.4.1 Interpretation of the ANOVA statistics.

Table 6 presents a summary of the factor analysis findings, detailing the F-values and p-values associated with each factor's impact on TS. The analysis indicates that GTE, which has an F-value of 0.4766 and a p-value of 0.5158, is not statistically significant, suggesting that the concentration of GTE does not have a meaningful effect on tensile strength. Similarly, BW exhibits an F-value of 1.6543 and a p-value of 0.2458, indicating that it also lacks a significant influence on TS, thereby implying that its variability has minimal individual effect. ZnO shows an F-value of 0.5162 and a p-value of 0.4995, further confirming the absence of a significant impact on TS. In contrast, GLY demonstrates an F-value of 4.5538 and a p-value of 0.0768, which is marginally significant, suggesting that glycerol may have a potential effect on tensile strength, warranting further investigation.

Table 7 provides an analysis of the interaction effects among various factors. The interaction between GTE and BW ($p = 0.8009$) indicates an absence of synergistic effects. The GTE and ZnO interaction ($p = 0.1644$) suggests some potential for interaction, although it is not statistically significant. The interaction between GTE and GLY ($p = 0.3336$) is regarded as a weak interaction. The BW and ZnO interaction ($p = 0.8052$) reveals minimal interaction, while the BW and GLY interaction ($p = 0.9092$) demonstrates a very weak effect. Finally, the interaction between ZnO and GLY ($p = 0.5772$) shows no significant interaction.

GLY seems to be the primary factor impacting tensile strength, although its influence is only marginally significant, just exceeding the 0.05 significance threshold. Other individual

Table 7 Interaction effect analysis

Interaction	p-Value	Interpretation
GTE × BW	0.8009	No synergistic effect
GTE × ZnO	0.1644	Shows some interaction potential
GTE × GLY	0.3336	Weak interaction
BW × ZnO	0.8052	Negligible interaction
BW × GLY	0.9092	Very weak effect
ZnO × GLY	0.5772	No significant interaction

Table 6 Factor analysis results

Factor	F-value	p-Value	Interpretation
GTE	0.4766	0.5158	Not significant. GTE concentration does not significantly affect tensile strength
BW	1.6543	0.2458	Not significant. BW (beeswax) variation has little individual effect
ZnO	0.5162	0.4995	Not significant. Zinc oxide does not independently influence TS
GLY	4.5538	0.0768	Marginally significant glycerol shows a potential effect; may warrant further investigation

factors and their interaction effects do not demonstrate statistical significance at the 95% confidence level. The analysis suggests that tensile strength is largely unaffected by most individual factors or their interactions, apart from GLY. Additional experiments or repetitions may provide further insight into the unclear or borderline effects, especially concerning GLY and the interaction between GTE and ZnO.

3.5 Summary of the design

In this research, the independent variables being examined are Green tea extract (from 0.5% to 2%), beeswax (0.5% to 1.5%), zinc oxide (0.05% to 1%), and glycerol (1% to 2%). Each variable is evaluated at five distinct levels: low (-1), medium (0), high (+1), plus alpha ($+\alpha$), and minus alpha ($-\alpha$). The response variables assessed include TS, EAB, WVP, MC, WS, L*, WI, YI, and OP. The design includes 14 experimental runs and 6 center points, totaling 20 trials designed to thoroughly explore the interactions among the factors and their influence on the response variables.

4 Model optimization and validation

4.1 Optimization of independent variables

1. Multi-criteria approach: optimization was carried out using a multi-criteria approach, meaning multiple response variables (like tensile strength, elongation at break, moisture content, *etc.*) were optimized simultaneously.

2. Derringer function/desirability function.

- This is a mathematical method used to find the best combination of independent variables.
- It transforms each response (such as tensile strength, elongation at break, *etc.*) into a dimensionless desirability scale (d_i) ranging from 0 (undesirable) to 1 (highly desirable).
- This helps in determining the best conditions for film formulation.

4.2 Desirability function application

Each response variable is given a desirability function, which means:

1. Desirable responses (things we want to increase):

- Tensile Strength (TS) – a higher tensile strength means a stronger film.
- Whiteness Index (WI) – a higher WI means a whiter film.
- Lightness (L*) – a higher value means the film is lighter in color.

2. Undesirable responses (things we want to decrease):

- Moisture Content (MC) – lower moisture content improves film stability.
- Elongation at break (EAB) – too much elongation may make the film too stretchy and weak.
- Water Vapor Permeability (WVP) – lower permeability makes the film more effective as a barrier.
- Water Solubility (WS) – a less soluble film is more stable under humid conditions.
- Yellowness Index (YI) – a lower YI means less yellowing of the film.
- Opacity (OP) – lower opacity makes the film more transparent.

The goal of optimization was to find the best combination of independent variables (BW, CEO, SP, *etc.*) that maximize the desirable properties and minimize the undesirable ones.

4.3 Optimization process

- Assigning goals: each response variable was assigned a goal (maximize or minimize).
- Setting independent variables in the range: the concentration levels of beeswax, clove essential oil, and other independent variables were adjusted within a specific range.
- Highest priority to all responses: instead of optimizing just one response, all were considered together.

4.4 Best condition selection

The combination of variables that gives the highest desirability index (close to 1) was chosen as the optimized condition.

4.5 Optimization process validation

Once the optimal conditions were identified:

- Experimental values (actual lab results) were compared with predicted values (from the optimization model).
- This ensures that the model's predictions are accurate and reliable.

4.6 Example

The Derringer desirability function is used to convert each response into a desirability score (0 to 1), where 0 means the response is completely undesirable and 1 means fully desirable. Each response is either maximized or minimized depending on gaols:

Maximize: TS, WI, and L* (higher values are better)

Minimize: MC, EAB, WVP, WS, YI, and OP (lower values are better)

Each response has a desirability function, which is a mathematical formula that assigns a desirability score based on whether the response meets the desired range.

4.6.1 Example of optimization using the desirability function. This example demonstrates how to optimize the composition of a chitosan-starch film incorporating GTE, BW, ZnO, and GLY using a multi-criteria approach known as the desirability function method.

5 Experimental design

Independent variables and their ranges are shown in Table 8. Table 8 which presents the ranges of the independent variables utilized in the experiments. The concentration of GTE varied from 0.5% to 2%, BW from 0.5% to 1.5%, ZnO from 0.05% to 1%, and GLY from 1% to 2%.

Table 8 Independent variable ranges

Variable	Range
Green tea extract (GTE)	0.5% to 2%
Beeswax (BW)	0.5% to 1.5%
Zinc oxide (ZnO)	0.05% to 1%
Glycerol (GLY)	1% to 2%

Table 9 Response variable categories

Category	Variables
Mechanical properties	Tensile Strength (TS) Elongation at break (EAB)
Barrier properties	Water Vapor Permeability (WVP) Moisture Content (MC) Water Solubility (WS)
Optical properties	Lightness (L*), Whiteness Index (WI), Yellowness Index (YI), and opacity (OP)

5.1 Response variables

Response variables according to their category are shown in Table 9 presenting the various categories of response variables assessed during the experiments.

5.2 Example data from one experimental run

The values of independent variables are given in Table 10.

All the experimental values and goals for optimization are mentioned in Table 11.

Table 11 presents the experimental data and optimization objectives for the response variables. The target for TS is to achieve a maximum value of 3.5 MPa. For EAB, the objective is to reduce the value to 150%. Additionally, the WVP, MC, and WS should be minimized, with experimental values recorded at 3.0×10^{-10}, 25%, and 30%, respectively. The WI and L* are to be maximized, with experimental values of 65 and 82, respectively. The YI should be minimized to 40, and OP should also be minimized to 1.1.

5.3 Transforming responses into desirability scores

Each response is transformed into a d_i ranging from 0 (undesirable) to 1 (highly desirable).

Desirability function types.For maximized responses (TS, WI, and L*):

$$d = \frac{X - X_{\min}}{X_{\max} - X_{\min}}$$

Table 10 Values of independent variables

Independent variables	Values
Green tea extract (GTE)	1.25%
Beeswax (BW)	1.0%
Zinc oxide (ZnO)	0.525%
Glycerol (GLY)	1.5%

Table 11 Experimental values and optimization goals for response variables

Response variable	Experimental value	Goal
TS	3.5 MPa	Max
EAB	150%	Min
WVP	3.0×10^{-10}	Min
MC	25%	Min
WS	30%	Min
WI	65	Max
YI	40	Min
L	82	Max
OP	1.1	Min

Table 12 Desirability scores for response variables

Response	Value	Desirability score (d_i)
TS (maximize)	3.5	0.33
EAB (minimize)	150	0.50
WVP (minimize)	3.0	0.67
MC (minimize)	25	0.42
WS (minimize)	30	0.50
WI (maximize)	65	0.60
YI (minimize)	40	0.50
L (maximize)*	80	0.50
OP (minimize)	1.1	0.57

For minimized responses (EAB, WVP, MC, WS, YI, and OP):

$$d = \frac{X_{\max} - X}{X_{\max} - X_{\min}}$$

Example desirability scores can be seen in Table 12.

Table 12 displays the desirability scores for the response variables derived from their experimental values. These scores are utilized to assess the proximity of the experimental outcomes to the optimal objective, whether it is to maximize or minimize. TS has a desirability score of 0.33, signifying that the current measurement of 3.5 MPa is relatively distant from the target aimed at maximizing this characteristic. EAB, recorded at 150%, possesses a desirability score of 0.50, indicating a moderate alignment with the desired minimum. WVP, measured at 3.0×10^{-10}, achieves a desirability score of 0.67, reflecting a comparatively favorable outcome towards the minimization goal. MC and WS both exhibit moderate desirability scores of 0.42 and 0.50, respectively, suggesting potential for enhancement in minimizing these attributes. The WI, with a score of 65, attains a desirability score of 0.60, demonstrating a strong alignment with the objective of maximizing this property. The YI, at 40, has a desirability score of 0.50, indicating that the result is midway towards the ideal minimum. Lightness, with a value of 80 and a desirability score of 0.50, suggests a balanced outcome in pursuing the maximization goal. Opacity (OP), with a score of 0.57, reflects moderate success in minimizing this property.

5.4 Calculating the overall desirability index

The overall desirability index (D) is computed as the geometric mean of all desirability scores:

$$D = (d_1 \times d_2 \times d_3 \times \cdots \times d_n)^{1/n}$$

For example:

$$D = (0.33 \times 0.5 \times 0.67 \times 0.42 \times 0.5 \times 0.6 \times 0.5 \times 0.5 \times 0.57)^{1/9}$$
$$\text{or, } D \approx 0.49$$

5.5 Selecting the optimal formulation

- A higher desirability index (close to 1) means the formulation is optimal.
- A low desirability index (closer to 0) suggests poor performance.
- The formulation with the highest D value across all experiments is selected as the best.

5.6 Response variable/mechanical properties

1. Tensile strength (TS) and elongation at break (EAB) which are mechanical properties of the films, specifically TS and EAB, were measured using the following formula:

$$\text{TS (MPa)} = \frac{\text{maximum force (N)}}{\text{cross-sectional area (mm}^2\text{)}}$$

$$\text{EAB (\%)} = \frac{\text{final length} - \text{initial length}}{\text{initial length}} \times 100$$

2. Moisture content (MC) and water solubility (WS) were assessed using a modified version of the standard hot air oven method. The moisture content was determined using the formula:

$$\text{Moisture content (\%)} = \frac{\text{initial weight} - \text{final weight}}{\text{initial weight}} \times 100$$

For the measurement of water solubility, the oven-dried film samples (initial weight = w_1) were submerged in 50 mL of distilled water at 25 °C for 24 hours, with occasional stirring. After the soaking period, the undissolved films were dried again at 90 °C for 24 hours and weighed (final weight = w_2). Water solubility was then calculated using the following equation:

$$\text{Water solubility (\%)} = \frac{(w_1 - w_2)}{w_3} \times 100$$

3. Color and optical parameters where the film's color was defined through CIELAB values: L* (lightness, ranging from 0 = black to 100 = white), a* (positive values indicate red, while negative values indicate green), and b* (positive values denote yellow, and negative values indicate blue). Using these values, the Whiteness Index (WI) and Yellowness Index (YI) were derived through the following formulae:

$$\text{WI} = 100 - \sqrt{(100 - L) + a^2 + b^2}$$

$$\text{YI} = 142.86 \times b$$

4. Opacity was assessed using rectangular samples measuring 4 × 40 mm which were positioned in a spectrophotometer cuvette, with an empty cuvette serving as the blank reference. Absorbance was measured at 600 nm, and opacity was determined using the following formula:

$$\text{OP} = \text{Abs}_{600}/d$$

where Abs_{600} = absorbance at 600 nm and d = film thickness (mm)

5.7 Characterization of optimized films

Different characterization studies will be employed to investigate the quality and basic properties of the optimized films. Antioxidant properties, thermal stability, and the structure, and purity of thin films can be understood using existing characterization studies like antioxidant activity, thermogravimetric analysis, SEM, FTIR and XRD, respectively.

1. The antioxidant properties of both the optimized film and the control film (pure SAE) were assessed through the DPPH free radical scavenging method. The DPPH scavenging activity was determined using the formula:

$$\text{DPPH scavenging activity (\%)} = \frac{(A_{\text{DPPH}} - A_{\text{S}})}{\text{ADPPH}} \times 100$$

where A_{DPPH} = absorbance of the DPPH solution without the sample and A_{S} = absorbance of the sample solution.

2. X-Ray Diffraction (XRD) determined the crystallinity, purity, and structural arrangement of the films.

3. Fourier Transform Infrared Spectroscopy (FTIR) was used to examine the attached functional groups with the films that lead to the absorption of specific frequency and provides information about bonding of different groups.

4. Thermogravimetric analysis (TGA) was used to investigate the thermal stability of the optimized film which was assessed with a thermogravimetric analyzer.

5. Scanning Electron Microscopy (SEM) was employed to investigate the surface and cross-sectional morphology of the composite films.

5.8 ANN modeling

Artificial Neural Networks (ANNs) are computational models inspired by the human brain, used for complex pattern recognition and predictive modeling. In this study, an ANN model was created to predict 9 response variables based on 3 input variables using MATLAB R2018a. ANNs are powerful tools that can capture complex, nonlinear relationships. In the development of biodegradable films, ANNs can be used to predict and

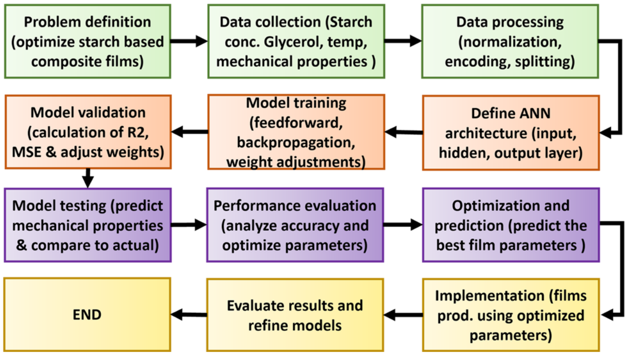

Fig. 4 Flow chart for artificial neural networks.

improve film properties based on variables like starch concentration, plasticizer levels, and processing conditions. The flowchart shown in Fig. 4 outlines the steps involved in developing and using an ANN model to optimize starch-based composite films, including stages such as problem identification, data processing, model training, validation, and execution.

- Table 13 presents the input and output variables used in the Artificial Neural Network (ANN) model.
- Data processing: to improve model performance, the dataset was preprocessed:

5.8.1 Normalization.

Data values were scaled between −1 and 1. This avoids large variations and helps in faster convergence during training.

Formula used for normalization:

$$X_{\text{scaled}} = \frac{X - X_{\min}}{X_{\max} - X_{\min}} \times 2 - 1$$

This makes sure that all variables contribute equally to the model.

5.8.2 Data splitting: (random splitting, stratified, and cross validation).

The dataset was divided into:

Training set (70%)-used to teach the neural network.

Test and validation set (30%)-used to evaluate model.

5.8.3 ANN architectural selection.

A multi-layer feed-forward ANN was designed, which consists of an input layer containing 4 input variables, hidden layers in which the number of neurons varied between 1 to 20, and the number of layers was 2, and an output layer which produced 9 predicted response values as shown in Fig. 5–7. The best number of neurons and layers was determined using Mean Squared Error (MSE).

Table 13 ANN model input and output variables

Inputs (IV – 4 factors)	Outputs (RV – 9 factors)
Beeswax (BW)	Tensile Strength (TS)
Glycerol (GLY)	Elongation at Break (EAB)
Zinc oxide (ZnO)	Water Vapor Permeability (WVP)
Green Tea Extract (GTE)	Moisture Content (MC)
—	Water Solubility (WS)
—	Whiteness Index (WI)
—	Yellowness Index (YI)
—	Lightness (L*)
—	Opacity (OP)

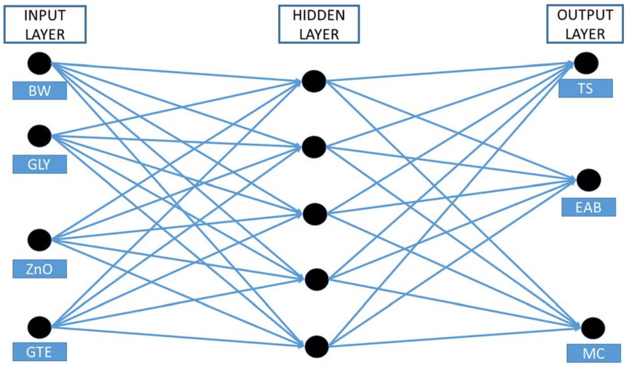

Fig. 5 Artificial Neural Networks (ANNs) including input factors to optimize the mechanical properties.

- Training the neural network: "training algorithm: back-propagation algorithm ("trainlm") was used.

Levenberg–Marquardt optimization was applied to update the weights and biases for faster convergence.

Learning function: "learngdm" (gradient descent with momentum weight & bias learning) was used to adjust the weight updates.

- Model evaluation after training, where the model's performance was measured using: Mean Squared Error (MSE): measures how close the predictions are to actual values:

$$\text{MSE} = \frac{1}{n}\sum_{i=n}^{n}(p_i - t_i)^2$$

where t_i represents experimental data, p_i represents predicted data, and n is the number of samples.

- Correlation coefficient (R): measures the strength of the relationship between experimental and predicted values:

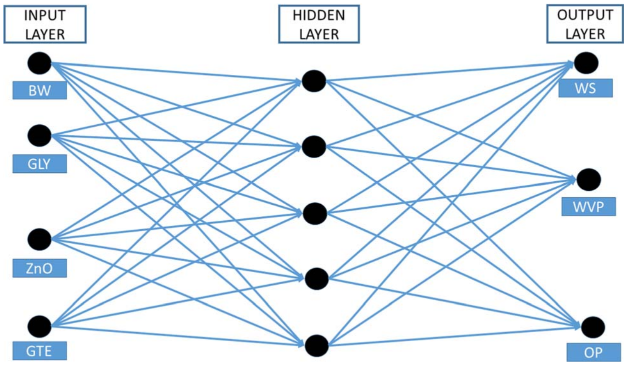

Fig. 6 Further derived components of films using Artificial Neural Networks (ANNs).

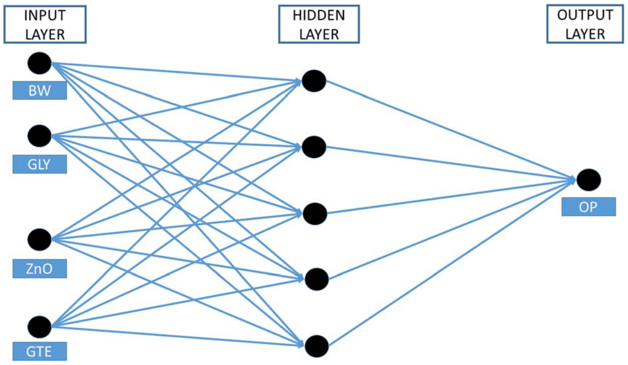

Fig. 7 Artificial Neural Network (ANN) optimized output.

$$R = \frac{\sum_{i=1}^{n}\left(t_i - \bar{t}\right)\left(p_i - \bar{p}\right)}{\sqrt{\sum_{i=1}^{n}\left(t_i - \bar{t}\right)^2} \times \sqrt{\sum_{i=1}^{n}\left(p_i - \bar{p}\right)^2}}$$

where $\bar{t}$ represents mean of experimental data and $\bar{p}$ represents mean of predicted data. If R is close to 1, the model predictions are highly accurate.

- Optimization of the model.

The ANN was trained multiple times, testing different neuron numbers and hidden layers. The best network was selected for the lowest MSE and highest R-value which was tested by comparing predicted values against actual experiment values.

5.9 Analysis of the developed model

Comparing prediction performance of RSM and ANN models.

This section describes how the performance of RSM and ANN models was compared using different statistical error metrics. let's go step by step.

1. Performance metrics used for comparison to determine which model (RSM or ANN) is better, the following metrics were calculated as shown in Table 14.

2. Mathematical equation for each metric.

Mean absolute error (MAE)

$$\text{MAE} = \frac{1}{n}\sum\left|p_i - t_i\right|$$

where p_i: predicted value (ANN or RSM), t_i: actual experimental value and n: total number of samples.

Goal: a lower MAE means the model's predictions are closer to the actual values.

Root mean squared error (RMSE)

$$\text{RMSE} = \sqrt{\frac{1}{n}\sum\left(p_i - t_i\right)^2}$$

Note: similar to MSE, but taking the square root makes the error comparable to the original data units.

Goal: a lower RMSE indicates better prediction accuracy.

Chi-square (χ^2)

$$\chi^2 = \sum\frac{\left(p_i - t_i\right)^2}{p_i}$$

Note: this metric compares actual and predicted values relative to the predicted values.

Goal: a lower χ^2 value indicates a better fit.

3. Interpreting the results, a higher χ^2 value indicates a better model having lower MAE, and RMSE values where χ^2 values indicate better predictive accuracy. If ANN has lower RMSE, MAE, and χ^2 than RSM, then ANN is the more accurate model.

When comparing Artificial Neural Networks (ANNs) with Response Surface Methodology (RSM), ANN consistently demonstrated superior performance across all assessed characteristics. This enhanced capability is due to ANN's proficiency in modeling complex, non-linear relationships among various input variables and their corresponding outputs. Although RSM is suitable for systems characterized by primarily linear or moderately quadratic interactions, it tends to be inadequate in addressing more complex, non-linear dependencies, an area where ANN thrives thanks to its layered structure and adaptive learning features.

6 Discussion & analysis

6.1 Tensile strength (TS) and elongation at break (EAB)

TS and EAB are key mechanical properties that affect the performance of edible and biodegradable films. High TS values are important for maintaining structural stability during handling, transportation, and storage.[51] This study showed that

Table 14 Model evaluation metrics and their objectives

Metric	Purpose	Goal for a good model
Coefficient of determination (R^2)	Measures how well the model explains the variability in data	Higher R^2 (closer to 1)
Mean Absolute Error (MAE)	Measures the average absolute error between predicted and actual values	Lower MAE
Root Mean Squared Error (RMSE)	Measures the square root of the average square error. Penalizes larger errors more than MAE.	Lower RMSE
Chi-square (χ^2)	Measures the difference between predicted and actual values, normalized by the predicted values	Lower χ^2

TS values were within the range reported in existing literature, with variations due to the interactions among the film's components. A two-factor interaction (2FI) model explained a significant portion of the variability, indicating that both individual and combined effects of the components can significantly influence the film's mechanical properties. In some cases, adding specific components disrupted the polymer matrix, resulting in reduced TS due to weaker intermolecular bonds.[52] Higher concentrations of certain hydrophobic or non-polar additives may have created heterogeneity, decreasing the film's cohesive strength.[53] However, in some instances, combining these components led to synergistic effects that improved mechanical performance, highlighting the complexity of formulation interactions.

Similarly, EAB values showed a wide range, comparable to that of biopolymer-based films and traditional synthetic materials such as polyethylene terephthalate (PET) and poly(vinyl alcohol-*co*-ethylene).[51,54,55] A quadratic model provided a strong statistical fit for the EAB data, showing that both linear and nonlinear interactions significantly influenced the film's flexibility. A decrease in EAB was observed in formulations with higher structural rigidity, likely due to restricted molecular movement within the polymer network.[56,57] Moreover, certain dispersed phases may have disrupted the film's continuity, leading to brittleness and reduced stretchability.[54]

6.2 Moisture content (MC)

MC plays a vital role in determining the barrier, thermal, and mechanical properties of biodegradable films. In this study, the observed MC values were consistent with those found in similar formulations. A quadratic regression model, with a coefficient of determination ($R^2 = 0.83$), successfully demonstrated the relationship between MC and the variables related to film composition. Statistical analysis through ANOVA showed that changes in the types and concentrations of components had a significant impact on MC levels ($p < 0.05$). Adding hydrophobic components to the predominantly hydrophilic polymer matrix resulted in a notable reduction in moisture retention. This decrease is attributed to the reduced water-binding capacity of the film, as hydrophobic additives generally repel moisture and reduce the film's affinity for water.[58] This finding emphasizes the need to balance hydrophilic and hydrophobic interactions during film formulation to achieve optimal moisture-related properties.

6.3 Water solubility

WS is a crucial characteristic of edible films, particularly those designed for high-moisture conditions where preserving structural integrity and product quality is important.[59] This research found that the solubility values of the films were within a range typical for protein-based edible films and were notably lower than those generally seen in polysaccharide-based films.[60,61] The response of WS to changes in formulation was most accurately represented by a quadratic regression model, achieving an R^2 value of 0.83. Several linear and quadratic terms were found to be statistically significant, suggesting intricate interactions among the formulation variables. The addition of hydrophobic components led to a reduction in WS, as these constituents decreased the film matrix's affinity for water by disrupting hydrogen bonding and promoting hydrophobic interactions.[62,63] Furthermore, certain additives with low hydrophilic-lipophilic balance (HLB) values further reduced solubility due to their limited compatibility with water, impeding effective interactions between the film matrix and aqueous environments.[64]

6.4 Water vapour permeability (WVP)

WVP is an essential factor that influences a film's ability to regulate moisture transfer, which is crucial for maintaining food quality and prolonging shelf life. In this research, the WVP values fell within the range documented for comparable biodegradable films, consistent with earlier studies.[65] The changes in WVP were accurately modeled using a second-order polynomial equation, which accounted for more than 90% of the variability in the data. Certain hydrophobic elements significantly decreased WVP by enhancing the film's resistance to moisture movement through improved barrier properties.[65] Notably, some additives exhibited concentration-dependent effects-initially enhancing barrier performance by increasing the tortuosity of the diffusion pathway, but ultimately undermining the film's structural integrity at higher concentrations, leading to increased WVP values.[66,67] Additionally, the synergistic effects of emulsifiers and plasticizers were found to enhance matrix cohesion and fortify hydrophobic regions, further improving moisture barrier properties.[68]

6.5 Color

Lightness (L*) plays a crucial role in determining consumer acceptance of edible films. This research utilized a quadratic regression model ($R^2 = 0.87$) to effectively illustrate the relationship between formulation variables and the L*. Certain ingredients were identified as enhancing lightness due to their natural optical properties, while others, especially those with darker or more saturated colors, negatively impacted lightness. Furthermore, second-order interactions and nonlinear effects contributed to additional decreases in lightness. The WI exhibited a similar trend, increasing with lighter-colored agents and decreasing with darker or chromophore-rich materials. Notably, some emulsifying agents displayed a negative relationship with the WI, possibly due to their effects on pigment distribution or polymer compatibility. The improvement of both L* and the WI in certain formulations is likely linked to the light-scattering properties of opaque components.[65] However, earlier studies indicate that the color response is significantly influenced by the composition and structure of the film matrix, as well as the characteristics of the added particles.[58,69] Conversely, films that included naturally pigmented compounds experienced a reduction in both lightness and whiteness, accompanied by a significant increase in the YI, likely due to their inherent color and the presence of light-absorbing phenolic compounds.[70]

6.6 Opacity

Opacity plays a vital role in assessing the appropriateness of packaging materials. A second-order regression analysis (R^2 = 86.31%) revealed that opacity is primarily affected by linear factors ($p < 0.005$). Certain additives can enhance opacity by obstructing light transmission through the film, likely due to the development of light-scattering structures within the material, a phenomenon corroborated by previous research.[71] On the other hand, the addition of different substances may compromise the dense structure of the film, resulting in reduced opacity and increased transparency. This effect may stem from these substances modifying the microstructure and potentially affecting the film's refractive index through interactions with water molecules, as noted by Gonzalez *et al.*[72] and Vargas *et al.*[73] Furthermore, specific emulsifiers have been shown to boost opacity, a finding consistent with earlier studies.[74,75]

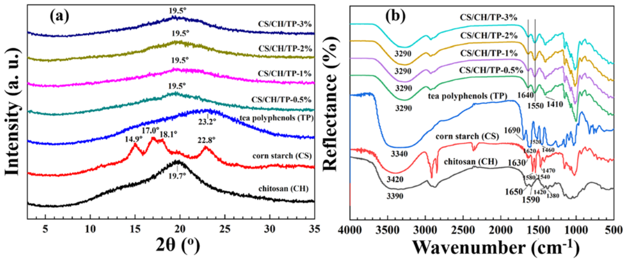

Fig. 8 (a) X-ray diffraction graph clearly illustrating the crystallinity changes in pure chitosan (CH), corn starch (CS), tea polyphenols (TP), and their composite films (CS/CH/TP-*x*%) as tea polyphenol content increases, and (b) Fourier transform infrared spectroscopy (FTIR) spectra of pure components-chitosan (CH), corn starch (CS), tea polyphenols (TP)-and their composite films with increasing concentrations of tea polyphenols (CS/CH/TP-0.5% up to CS/CH/TP-3%).[83] Adapted from Open access under the Creative Commons BY license. Copyright 2021 MDPI.

6.7 Optimized film characterization

6.7.1 Antioxidant activity. Antioxidant activity is an essential characteristic of edible films, as it helps reduce the detrimental effects of free radicals in both food products and biological systems.[76] The commonly utilized DPPH assay serves as a dependable method for assessing the free radical scavenging ability of a material, which is directly related to its potential for prolonging the shelf life of packaged foods.[77] In this study, both the standard film and its optimized version demonstrated inherent antioxidant properties. The activity of the standard sample is attributed to the natural free radical scavenging capabilities of its primary polymer matrix, while the improved performance of the optimized film is associated with the addition of natural bioactive compounds. These compounds, which are typically abundant in phenolic structures, are recognized for their significant role in neutralizing free radicals, thus enhancing the overall antioxidant capacity.[13,78]

6.7.2 X-ray diffraction (XRD) analysis. The XRD analysis was performed to assess the structural arrangement and crystallinity of the optimized film. The resulting diffraction pattern revealed a semi-crystalline character, exhibiting both amorphous and crystalline regions. A broad peak centered at approximately 20° was associated with the amorphous characteristics of the soy protein matrix, specifically linked to the presence of 7S and 11S amorphous globulins, which are typical components of soy protein structures.[79,80] Conversely, several sharp and well-defined peaks observed at both lower and higher diffraction angles, including those near 5.5°, 6.4°, 15.9°, 23.1°, 27.7°, and 34.8°, indicated the presence of crystalline domains within the film. These peaks were primarily attributed to the addition of beeswax, which is recognized for its contribution to the crystalline structure due to its orderly molecular configuration. The emergence of these peaks signifies a favorable level of molecular organization and implies that the beeswax was effectively integrated into the film matrix. The degree of crystallinity observed is also affected by the physical processing conditions, particularly during the cooling and drying phases, which influence the alignment and packing of molecules throughout the film formation process. These structural characteristics not only validate the compatibility of the film-forming components but also indicate robust intermolecular interactions that are essential for the mechanical strength and barrier properties of the final film.[81,82]

Fig. 8(a) shows the XRD patterns of the chitosan (CH), corn starch (CS), tea polyphenols (TP), and their composite films (CS/CH/TP-*x*%) in a brief study done by Gao *et al.*[83] The diffraction peaks for chitosan exhibited a broad peak at 19.7°, indicating a predominance of amorphous regions, which is common for chitosan due to its flexible polymer chains. Corn Starch (CS) showed sharp peaks at 14.9°, 17.0°, 18.1°, and 22.8°, indicating an A-type crystalline structure and a higher degree of crystallinity, whereas tea polyphenols (TP) had a very broad and weak peak at 23.2°, suggesting an amorphous or poorly crystalline nature. Composite films (CS/CH/TP-*x*%), regardless of TP concentration, show a single broad peak at 19.5°, with the disappearance of starch's sharp crystalline peaks. This indicated a significant decrease in overall crystallinity and the formation of a more amorphous structure. The absence of new peaks and the broadening of the main peak suggested strong molecular interactions (such as hydrogen bonding) between chitosan, starch, and tea polyphenols. These interactions disrupted the regular crystalline arrangement of starch and chitosan, leading to a homogeneous amorphous matrix.

6.7.3 Fourier transform infrared spectroscopy (FTIR) analysis. FTIR is an advanced analytical method employed to identify chemical bonds and functional groups within materials by examining their absorption of infrared (IR) light. When subjected to IR radiation, the molecules of a material absorb specific frequencies, leading to vibrational movements in the bonds, such as stretching, bending, or twisting. These unique absorption patterns generate a distinct spectral "fingerprint" for the material. As noted by Coates[84] a key reference for interpreting IR spectra is that, each type of chemical bond (such as O–H, C–H, C=O, N–H, *etc.*) absorbs infrared radiation at specific wavenumbers (expressed in cm^{-1}). By scrutinizing these absorption bands, researchers can identify the functional groups present in a given sample. Various researchers have studied the application of FTIR in the study of natural polymers, specifically starch. Their findings indicated that starch displays consistent IR absorption bands, which correlate with its molecular structure, thereby aiding in the evaluation of its composition and the detection of any modifications.

The FTIR spectra shown in Fig. 8(b) illustrated the reflectance of various films[83] where wavenumbers between 3290–3340 cm^{-1} were attributed to broad O–H and N–H stretching indicating the presence of hydroxyl (from starch and polyphenols) and amino groups (from chitosan). The persistence of this peak in all composite films suggests that hydrogen bonding remains a dominant interaction, and the blending process does not disrupt these functional groups. Amide I and II bands at 1640–1690 cm^{-1} and 1550 cm^{-1} were associated with C=O stretching and N–H bending, respectively, both characteristic of protein and polysaccharide matrices. The composite films sometimes shifted as compared to pure components, indicating interactions (likely hydrogen bonding or electrostatic) between chitosan, starch, and tea polyphenols. The shift towards lower wavenumbers upon TP addition is evidence of strong intermolecular interactions, likely due to the aromatic rings and hydroxyl groups in polyphenols forming new hydrogen bonds with the matrix. Peaks in the 1470–1410 cm^{-1} region were attributed to –CH$_2$ bending and –CH$_3$ symmetrical deformation. The presence and intensity of these peaks in the composite films confirmed the integration of chitosan and starch, and their modification, as TP concentration increases suggest changes in the microstructure and packing of the polymer chains. Furthermore, the fingerprint region below 1500 cm^{-1} represented the C–O, C–C, and C–H bending vibrations that changed according to TP concentration reflecting successful incorporation and molecular interaction of TP within the CS/CH matrix.

In a similar vein, Lii *et al.*[85] employed FTIR to explore the structure of xanthan gum, a type of polysaccharide. Their research validated the effectiveness of FTIR in identifying characteristic functional groups within complex carbohydrates, which is instrumental in understanding molecular conformation and interactions with other substances. Additionally, FTIR was used to examine glycerol, a simple polyol compound. Their results underscored the capability of FTIR to identify hydroxyl (–OH) groups and other molecular characteristics in small organic molecules, proving valuable for the analysis of additives or plasticizers in biopolymer systems.

6.7.4 Thermogravimetric analysis (TGA). TGA was utilized to assess the thermal stability and decomposition characteristics of the developed films. This method also sheds light on how composite interactions affect film stability when subjected to thermal stress.[86] The TGA results for the optimized film revealed the correlation between mass loss and temperature, while the derivative thermogravimetric (DTG) curve depicted the rate of weight change during the heating process. Thermal degradation was observed to occur in three distinct phases. The first phase, occurring between 25 °C and approximately 112 °C, was primarily characterized by the evaporation of free moisture and the loss of minor volatile components. The second phase, which extended to around 243 °C, exhibited a significant mass reduction of approximately 28.96%. This reduction can be linked to the degradation of low molecular weight additives, partial breakdown of structural polymers, and the evaporation of plasticizers.[87–89] The final phase, occurring between 243 °C and 363 °C, involved the thermal decomposition of high molecular weight compounds and the evaporation of bound water, resulting in a sharp decrease in sample mass.[90]

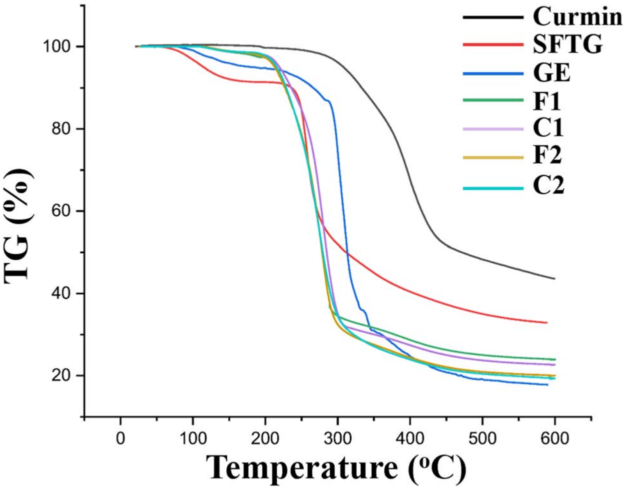

Fig. 9 Thermogravimetric analysis (TGA) of pure curmin, SFTG, GE, and several film formulations (F1, F2, C1, and C2).[91] Adapted from open access under the Creative Commons BY license. Copyright 2022 MDPI.

The TGA curves depicted in the accompanying Fig. 9 demonstrate the thermal stability of various films studied by Amani *et al.*[91] It could be observed that pure curcumin (curmin) displays the highest thermal stability, with major weight loss starting at around 270 °C and significant residue remaining even above 400 °C. SFTG (tragacanth gum) and GE (Gelatin) degraded at lower temperatures than curcumin, 220 °C and 260–450 °C, respectively. All film samples F1 (1GE:1SFTG), F2 (2GE:1SFTG), C1 (1GE:1SFTG/curcumin), and C2(2GE:1SFTG/curcumin) showed similar degradation profiles, with the main weight loss (about 70%) occurring between 200–300 °C, attributed to polymer depolymerization. The final decomposition stage (about 10% mass loss) is due to the breakdown of the remaining film components. The films have lower thermal stability than pure curcumin, consistent with the observation that blending curcumin with biopolymers reduces thermal stability. The order of thermal stability was found to be curmin >GE ≈ F1 ≈ F2 ≈ C1 ≈ C2 > SFTG, with all film samples clustering closely together.

6.7.5 Scanning electron microscopy (SEM) analysis. SEM was utilized to examine the microstructural arrangement and compatibility of the various elements within the composite film. This analysis yielded crucial information regarding both the internal and surface morphology, which are vital for assessing mechanical strength and barrier efficacy.[58] The film's surface displayed significant roughness and irregularities, likely resulting from the recrystallization and accumulation of hydrophobic particles during the drying phase. These particles disrupted the uniformity of the matrix, leading to a coarse and uneven texture.[82] Such morphological characteristics can impact both optical clarity and surface integrity.

Internally, microporous structures were identified, possibly formed by the evaporation of volatile substances during the film casting process. The distribution of lipophilic droplets appeared to be well integrated within the continuous polymer matrix, creating distinct regions that contributed to a loosely arranged internal structure. While this porosity may enhance breathability, it could also influence moisture barrier properties based on the overall density and connectivity of the pores.[90] Despite the observed rough surface textures and internal porosity, the composite film exhibited a consistent distribution of all components, with no signs of phase separation or significant aggregation. This structural uniformity indicates effective miscibility and interaction among the film-forming agents, likely facilitated by ultrasonication and emulsifying agents. The resulting homogeneity within the matrix promotes improved mechanical cohesion and functional stability of the composite film.[70]

7 Conclusion

The development of biodegradable edible films made from natural biopolymers, bioactive additives, and nanomaterials provides an eco-friendly alternative to conventional plastic packaging. This review highlights significant improvements in the mechanical, barrier, and antimicrobial properties of these films, achieved by incorporating natural polymers such as starch, chitosan, and essential oils, along with bioactive compounds like zinc oxide nanoparticles. Advanced optimization techniques, including Response Surface Methodology (RSM) and Artificial Neural Networks (ANNs), have been instrumental in fine-tuning film formulations to meet specific performance criteria. The inclusion of bioactive agents such as green tea extract and beeswax not only enhances the antioxidant and antimicrobial properties of the films but also improves their mechanical strength and moisture resistance. Characterization methods like FTIR, SEM, and XRD have confirmed the structural integrity and functional compatibility of the films, while AI-driven optimization models have demonstrated superior predictive accuracy compared to traditional techniques. Besides this, the AI models can be incorporated to develop other bio-based films. These interdisciplinary innovations pave the way for sustainable, high-performance food packaging solutions that align with sustainability goals. Future research should focus on scaling production, assessing real-world biodegradability, and addressing regulatory challenges to accelerate the commercialization of these groundbreaking bio-based films. Despite promising laboratory results, the absence of shelf-life and antimicrobial testing on actual food products limits the practical validation of these films. Therefore, further studies are needed to determine whether the existing models can be applied to different biopolymer combinations and food packaging applications. Before the widespread use and commercialization of these films, it is crucial to conduct real-world food testing and evaluate these models with other natural materials.

Author contributions

SG did conceptualization, formal analysis, funding acquisition, investigation, methodology, project administration, supervision, validation, visualization, writing – review & editing; MV did data curation, formal analysis, investigation, methodology, validation, writing – original draft; TL(lead) did data curation, formal analysis, methodology, and writing – original draft.

Conflicts of interest

There are no conflicts to declare.

Data availability

No primary research results, software or code have been included and no new data were generated or analysed as part of this review.

Acknowledgements

MV acknowledges the research project under DST INSPIRE Fellowships 2024, with Inspire code IF230126.

Notes and references

1 A. Travalini, I. Demiate and B. Lamsal, in *Bioplastics and Biocomposites: A Practical Introduction*, Royal Society of Chemistry, 2023.
2 S. Khadsai, R. Janmanee, P. Sam-Ang, Y. Nuanchawee, W. Rakitikul, W. Mankhong, W. Likittrakulwong and P. Ninjiaranai, *Polymers*, 2024, **16**, 1647.
3 A. Kumar, P. P. Srivastav, M. Pravitha, M. Hasan, S. Mangaraj, D. K. Verma, *et al.*, *Food Packag. Shelf Life*, 2022, **31**, 100778.
4 C. Fragassa, A. Pesic, S. Mattiello, A. Pavlovic and C. Santulli, *J. Mar. Sci. Eng.*, 2025, **13**, 177.
5 I. Solihat, S. R. Setyawati, L. Sulistiawaty, M. F. Khoirurrizal, *et al.*, *Jurnal Kimia Riset*, 2023, **8**, 49–58.
6 A. Younes, M. Li and S. Karboune, *Crit. Rev. Food Sci. Nutr.*, 2023, **63**, 9111–9135.
7 X. Wang, X. Li, H. Feng, H. Peng and G. Ma, *Acta Mater. Compositae Sin.*, 2022, 2907–2917.
8 C. Du, F. Jiang, W. Jiang, W. Ge and S.-k. Du, *Int. J. Biol. Macromol.*, 2020, **164**, 1785–1793.
9 M. Shobha and R. Tharanathan, *Food Hydrocolloids*, 2009, **23**, 749–754.
10 X. Wang, Y. Du, J. Luo, J. Yang, W. Wang and J. F. Kennedy, *Carbohydr. Polym.*, 2009, **77**, 449–456.
11 C. Vásquez, G. Henríquez, J. V. López, E. K. Penott-Chang, A. J. Sandoval and A. J. Müller, *LWT–Food Sci. Technol.*, 2019, **111**, 744–750.

12 L. Wang, R. Wang, F. Chen, T. Jiang, H. Wang, M. Slavik, H. Wei and Y. Li, *Food Chem.*, 2017, **221**, 776–782.

13 A. G. Al-Hashimi, A. B. Ammar, F. Cacciola and N. Lakhssassi, *Foods*, 2020, **9**, 184.

14 J. Zhang, C. Cao, S. Zheng, W. Li, B. Li and X. Xie, *Food Packag. Shelf Life*, 2020, **24**, 100487.

15 M. Intelligence, *Smart Packaging Market Size, Companies, Share, Trends, Growth & Industry Analysis (2025 - 2030)*, 2025.

16 V. Schmidt, C. Giacomelli, M. S. Soldi and V. Soldi, *Macromol. Symp.*, 2005, 127–137.

17 G. E. Box and K. B. Wilson, in *Breakthroughs in Statistics: Methodology and Distribution*, Springer, 1992, pp. 270–310.

18 A. Cassano, C. Conidi and E. Drioli, *J. Food Eng.*, 2011, **107**, 366–373.

19 M. Zaccone, M. K. Patel, L. De Brauwer, R. Nair, M. L. Montalbano, M. Monti and K. Oksman, *Polymers*, 2022, **14**, 562.

20 Z. Cui, Y. Li, X. Feng and Z. Hu, *J. Food Process. Preserv.*, 2023, **2023**, 3578799.

21 A. L. Charles, N. Motsa and A. A. Abdillah, *Polymers*, 2022, **14**, 3462.

22 J. Simona, D. Dani, S. Petr, N. Marcela, T. Jakub and T. Bohuslava, *Polymers*, 2021, **13**, 332.

23 C. Togas, S. Berhimpon, R. I. Montolalu, H. A. Dien and F. Mentang, *J. Pengolah. Has. Perikan. Indones.*, 2017, **20**, 468–477.

24 B. Girgin, M. Abahuni Ucÿar, E. Moroydoĺr Derun and N. Tugrul, *ACS Food Sci. Technol.*, 2024, **5**, 75–84.

25 E. Butnaru, E. Stoleru, M. A. Brebu, R. N. Darie-Nita, A. Bargan and C. Vasile, *Materials*, 2019, **12**, 373.

26 M. Verma and S. Gautam, *Sustainable Energy Fuels*, 2025, **9**, 3203.

27 R. H. Myers, D. C. Montgomery and C. M. Anderson-Cook, *Response Surface Methodology: Process and Product Optimization Using Designed Experiments*, John Wiley & Sons, 2016.

28 D. C. Montgomery, *Design and Analysis of Experiments*, John wiley & sons, 2017.

29 D. Baş and İ. H. Boyacı, *J. Food Eng.*, 2007, **78**, 836–845.

30 M. K. Chatli, R. V. Wagh, N. Mehta, P. Kumar and O. P. Malav, *Nutr. Food Sci.*, 2021, **51**, 205–221.

31 M. A. Bezerra, R. E. Santelli, E. P. Oliveira, L. S. Villar and L. A. Escaleira, *Talanta*, 2008, **76**, 965–977.

32 S. Haykin, *Neural Networks and Learning Machines, 3/E*, Pearson Education India, 2009.

33 V. B. Mohan, K.-t. Lau, D. Hui and D. Bhattacharyya, *Composites, Part B*, 2018, **142**, 200–220.

34 S. Díaz-Sánchez, S. Sánchez, M. Sánchez, S. Herrera-León, I. Hanning and D. Vidal, *Int. J. Food Microbiol.*, 2012, **160**, 179–182.

35 C. Cortes and V. Vapnik, *Mach. Learn.*, 1995, **20**, 273–297.

36 E. Gallego, F. Roca, J. Perales and X. Guardino, *Talanta*, 2011, **85**, 662–672.

37 J. R. Quinlan, *Mach. Learn.*, 1986, **1**, 81–106.

38 L. Breiman, *Mach. Learn.*, 2001, **45**, 5–32.

39 W. Lin, Y. Ni and J. Pang, *Int. J. Biol. Macromol.*, 2020, **149**, 853–860.

40 Y. LeCun, Y. Bengio and G. Hinton, *Nature*, 2015, **521**, 436–444.

41 A. Kamilaris and F. X. Prenafeta-Boldú, *Comput. Electron. Agric.*, 2018, **147**, 70–90.

42 M. Polomoshnov, K.-M. Reichert, L. Rettenberger, M. Ungerer, G. Hernandez-Sosa, U. Gengenbach and M. Reischl, *J. Intell. Manuf.*, 2024, 1–18.

43 T. Cover and P. Hart, *IEEE Trans. Inf. Theor.*, 1967, **13**, 21–27.

44 N. S. Altman, *Am. Statistician*, 1992, **46**, 175–185.

45 A. Sirelkhatim, S. Mahmud, A. Seeni, N. H. M. Kaus, L. C. Ann, S. K. M. Bakhori, H. Hasan and D. Mohamad, *Nano-Micro Lett.*, 2015, **7**, 219–242.

46 I. Ahmad, M. Y. Alshahrani, S. Wahab, A. I. Al-Harbi, N. Nisar, Y. Alraey, A. Alqahtani, M. A. Mir, S. Irfan and M. Saeed, *J. King Saud Univ. Sci.*, 2022, **34**, 102110.

47 D. Carrizo, G. Taborda, C. Nerín and O. Bosetti, *Innov. Food Sci. Emerg. Technol.*, 2016, **33**, 534–541.

48 A. A. Barzegaran, M. Jokar and D. M. Javanmard, *J. Mach. Learn.*, 2014, **15**, 2869–2909.

49 S. F. Hosseini, Z. Mousavi and D. J. McClements, *Food Chem.*, 2023, **424**, 136404.

50 Y. A. Shah, S. Bhatia, A. Al-Harrasi, M. Tarahi, H. Almasi, R. Chawla and A. M. M. Ali, *Int. J. Biol. Macromol.*, 2024, 132354.

51 R. Georgiou and R. Kostovska, *Maso Int. J. Food Sci. Technol.*, 2022, **12**, 25–33.

52 E. Athanasopoulou, F. Bigi, E. Maurizzi, E. I. E. Karellou, C. S. Pappas, A. Quartieri and T. Tsironi, *Sci. Rep.*, 2024, **14**, 517.

53 R. Ghadermazi, S. Hamdipour, K. Sadeghi, R. Ghadermazi and A. Khosrowshahi Asl, *Food Sci. Nutr.*, 2019, **7**, 3363–3377.

54 W. Blel, P. Legentilhomme, T. Bénézech, J. Legrand and C. Le Gentil-Lelièvre, *J. Food Eng.*, 2009, **90**, 433–440.

55 S. Jain and A. K. Anal, *Food Res. Int.*, 2018, **103**, 234–242.

56 S. Isaka, K. Cho, S. Nakazono, R. Abu, M. Ueno, D. Kim and T. Oda, *Int. J. Biol. Macromol.*, 2015, **74**, 68–75.

57 A. Wang, J. Lin and Q. Zhong, *Food Hydrocolloids*, 2021, **113**, 106469.

58 P. Klangmuang and R. Sothornvit, *Food Hydrocolloids*, 2016, **61**, 609–616.

59 J. Zheng, C. Li, X. Wu, M. Liu, X. Sun, Y. Yang, M. Hao, S. Sheng, Y. Sun, H. Zhang, *et al.*, *Int. J. Biol. Macromol.*, 2014, **64**, 106–110.

60 Z. M. Adilah, B. Jamilah and Z. N. Hanani, *Food Hydrocolloids*, 2018, **74**, 207–218.

61 H. Liu and D. Chaudhary, *Carbohydr. Polym.*, 2013, **98**, 391–396.

62 P. L. Kashyap, X. Xiang and P. Heiden, *Int. J. Biol. Macromol.*, 2015, **77**, 36–51.

63 N. Cordeiro, M. Faria, E. Abraham and L. A. Pothan, *Carbohydr. Polym.*, 2013, **98**, 1065–1071.

64 R. Milani, L. Pirrie, L. Gazzera, A. Paananen, M. Baldrighi, E. Monogioudi, G. Cavallo, M. Linder, G. Resnati and P. Metrangolo, *J. Colloid Interface Sci.*, 2015, **448**, 140–147.

65 J. A. C. Vilca, B. S. Ortiz-Quispe, C. R. Apaza-Cusiatau, E. M. de Jara, M. J. Quequezana-Bedregal, E. E. Gutierrez-

Oppe and P. de Alcântara Pessôa Filho, *SN Appl. Sci.*, 2023, **5**, 370.

66 S. Shojaee-Aliabadi, H. Hosseini, M. A. Mohammadifar, A. Mohammadi, M. Ghasemlou, S. M. Ojagh, S. M. Hosseini and R. Khaksar, *Int. J. Biol. Macromol.*, 2013, **52**, 116–124.

67 J. Bonilla, L. Atarés, M. Vargas and A. Chiralt, *Food Hydrocolloids*, 2012, **26**, 9–16.

68 M. d. C. M. Serrano, R. Santos, C. Viegas, M. M. Sapata, R. G. Santos, J. Condeço, A. C. Marques and J. C. Bordado, Starch-Based Edible Films Properties and Sensory Evaluation for Food Applications, available at SSRN: **https://ssrn.com/abstract=3910229** or DOI: **10.2139/ssrn.3910229**.

69 F. M. Monedero, M. J. Fabra, P. Talens and A. Chiralt, *J. Food Eng.*, 2009, **91**, 509–515.

70 O. Gul, F. T. Saricaoglu, A. Besir, I. Atalar and F. Yazici, *Ultrason. Sonochem.*, 2018, **41**, 466–474.

71 M. J. Fabra, P. Talens and A. Chiralt, *Food Hydrocolloids*, 2009, **23**, 676–683.

72 L. Sánchez-González, M. Vargas, C. González-Martínez, A. Chiralt and M. Cháfer, *Food Hydrocolloids*, 2009, **23**, 2102–2109.

73 M. Vargas, A. Albors, A. Chiralt and C. González-Martínez, *Food Hydrocolloids*, 2009, **23**, 536–547.

74 C. Andreuccetti, R. A. Carvalho, T. Galicia-García, F. Martínez-Bustos and C. R. Grosso, *J. Food Eng.*, 2011, **103**, 129–136.

75 D. Carpiné, J. L. A. Dagostin, E. F. de Andrade, L. C. Bertan and M. R. Mafra, *Ind. Crops Prod.*, 2016, **83**, 364–371.

76 Y. Pan, K. Wang, S. Huang, H. Wang, X. Mu, C. He, X. Ji, J. Zhang and F. Huang, *Food Chem.*, 2008, **106**, 1264–1270.

77 M. Jridi, S. Boughriba, O. Abdelhedi, H. Nciri, R. Nasri, H. Kchaou, M. Kaya, H. Sebai, N. Zouari and M. Nasri, *Food Packag. Shelf Life*, 2019, **21**, 100342.

78 S. T. Baghbadorani, M. R. Ehsani, M. Mirlohi, H. Ezzatpanah, L. Azadbakht and M. Babashahi, *Adv. Biomed. Res.*, 2017, **6**, 62.

79 X. Liu, H. Kang, Z. Wang, W. Zhang, J. Li and S. Zhang, *Materials*, 2017, **10**, 653.

80 S. Pattanaik, A. K. Sutar and T. Maharana, *IOP Conf. Ser.:Mater. Sci. Eng.*, 2018, 012011.

81 C. Valenzuela, L. Abugoch and C. Tapia, *LWT–Food Sci. Technol.*, 2013, **50**, 531–537.

82 R. Zhang, W. Wang, H. Zhang, Y. Dai, H. Dong and H. Hou, *Food Hydrocolloids*, 2019, **88**, 283–290.

83 L. Gao, T. Zhu, F. He, Z. Ou, J. Xu and L. Ren, *Coatings*, 2021, **11**, 817.

84 J. Coates, *et al.*, *Encyclopedia Anal. Chem.*, 2000, **12**, 10815–10837.

85 C.-Y. Lii, S. Liaw, V.-F. Lai and P. Tomasik, *Eur. Polym. J.*, 2002, **38**, 1377–1381.

86 A. Nouri, M. T. Yaraki, A. Lajevardi, T. Rahimi, M. Tanzifi and M. Ghorbanpour, *Food Packag. Shelf Life*, 2020, **23**, 100435.

87 K. Feng, P. Wen, H. Yang, N. Li, W. Y. Lou, M. H. Zong and H. Wu, *RSC Adv.*, 2017, **7**, 1572–1580.

88 A. González and C. I. A. Igarzabal, *Food Hydrocolloids*, 2013, **33**, 289–296.

89 X. Chen, F. Cui, H. Zi, Y. Zhou, H. Liu and J. Xiao, *Int. J. Biol. Macromol.*, 2019, **141**, 1175–1182.

90 Y. Xu, Y. Chu, X. Feng, C. Gao, D. Wu, W. Cheng, L. Meng, Y. Zhang and X. Tang, *Int. J. Biol. Macromol.*, 2020, **156**, 111–119.

91 F. Amani, A. Rezaei, H. Akbari, C. Dima and S. M. Jafari, *Foods*, 2022, **11**, 3168.